Article:
Aldakheel, F., Ismail, M.S., Hughes, K.J. et al. (2020) Gas permeability, wettability and morphology of gas diffusion layers before and after performing a realistic ex-situ compression test. Renewable Energy, 151. pp. 1082-1091. ISSN: 0960-1481

https://doi.org/10.1016/j.renene.2019.11.109

Abstract

The through-plane gas permeability, wettability, thickness and morphology have been investigated before and after a compression test, which is important to the GDL design. The compression tests were designed to simulate the initial assembling compression and the cycles of loading and unloading arising as a result of hydration/dehydration of the membrane. Owing to the presence of the microporous layer (MPL), the results show that the coated gas diffusion layers (GDLs) are slightly more resistive to deformation than the uncoated GDLs. Amongst all the tested carbon substrates (i.e. the uncoated GDLs), Toray carbon substrate was found to show the least reduction in thickness and gas permeability after compression, and this was attributed to its relatively high density and low porosity. As for the coated GDLs, the level of MPL penetration for one of the tested GDLs (i.e. SGL 35BC) was significantly higher than that of the other GDL (i.e. SGL 34BC), resulting in substantially less reduction in thickness and gas permeability of the former GDL after compression. Finally, the contact angles of all the tested GDL materials were found to decrease after compression due to the decreased surface roughness.

Keywords: PEM fuel cells; Gas diffusion layers; Compression; Gas permeability; Contact angle; MPL penetration

1. Introduction

Proton exchange membrane (PEM) fuel cells (or Polymer Electrolyte Fuel Cells (PEFCs)) are energy converters that directly convert chemical energy stored in hydrogen fuel into electrical energy. In the last two decades, PEM fuel cell technology has gained a good deal of attention and this is primarily due to its high efficiency, low operating temperature, and consequent rapid start-up [1]–[4]. Gas diffusion layers, placed between the flow field plates and the catalyst layers, are key components in PEM fuel cells; they enhance the uniformity of the distribution of the reacting gases over the catalyst layer and assist in removing excess liquid water [5], [6]. Typically, GDLs are made of either woven carbon or non-woven carbon fibers. Each type of GDL has its own characteristics and limits with regards to the porosity, diffusivity, mechanical properties and gas permeability.

The lifetime and the durability of the GDL is an important aspect that affects the overall performance of the PEM fuel cell and is closely correlated to the properties of its main components [7]. Generally, there are two types of degradation that significantly deteriorate the functions of the GDL and in turn the performance of the PEM fuel cell namely, chemical degradation and mechanical degradation. Briefly, the chemical degradation is attributed to the corrosion and erosion of the carbon loading, as well as the wetting characteristics of the polytetrafluoroethylene (PTFE) available in the GDL. On the other hand, the mechanical degradation is attributed to two main sources, namely; (i) the compression while assembling the fuel cell, and (ii) the cyclic compression due to the hygrothermal effects [8]. Much research has been conducted on the compression effects on the overall performance of PEM fuel cells [9]–[12], and the electrical contact resistance between various fuel cell components [13]–[17]. For instance, Escribano et al. [18] conducted an experimental investigation to evaluate the compressibility of different types of GDL samples using a universal testing machine

(INSTRON 4450). They used a stack of 10 GDL samples in order to minimise the error associated with the measurement of the GDL thickness during compression. However, using a stack of multiple GDL samples can lead to inaccuracy in determining the actual thickness of each GDL sample after compression.

The clamping force used to assemble the fuel cell significantly affects its performance and it needs to be optimized to ensure (i) good electrical contact between the various components of the fuel cell and (ii) adequate supply of reacting gases to the catalyst layer. Xing et al. [19] conducted a numerical study to determine the optimum clamping pressure value under different operating voltages. They found that a range of 1.0-1.5 MPa of clamping pressure is optimum as it results in reasonably low contact resistance and an adequate supply of reactants to the catalyst layer. This is in line with the recommendation of the US Department of Energy (DoE) that the compression on the fuel cell be 1.4 MPa [20], [21].

However, at low fuel cell voltages, the rate of chemical reactions is higher and therefore higher amounts of reactants are required. In this case, the clamping pressure needs to be relatively low (e.g. 0.8 MPa) to allow more reactant gases to reach the reactive areas in the catalyst layer especially under the areas beneath the ribs of the flow-field plates [19]. Notably, only a few studies have investigated the effects of cyclic compression, arising as a result of the hygrothermal effects, on the GDL material. For instance, Gigos et al. [22] experimentally and numerically investigated the effects of cyclic compression in the range of 0-12 MPa on 3 different types of GDL materials. They found that the deformation is irreversible after the first loading.

Radhakirshnan and Haridoss [23] conducted an experiment to analyse the impact of cyclic compression on the GDL material at two different ranges: 0-1.7 MPa and 0-3.4 MPa. The GDL material used in their study was Toray paper (TGP-H-120), and it was compressed using a pair

of aluminum end plates with two graphite plates between which the GDL is sandwiched. They found that, as a result of the applied cyclic compression, a permanent deformation in the GDL structure occurs. This change in the structure has a direct impact on other GDL properties: surface roughness, electrical resistance, GDL thickness and in-plane permeability. Mason et al. [13] similarly conducted a study on the effect of cyclic compression on a Toray GDL material using a commercial compression-controlled unit cell. They studied the effects of cyclic compression on the thickness and the electrical resistance of the GDL materials. It was found that the deformation of the tested GDL becomes permanent after 10 cycles. The compression, either steady-state or cyclic, affects the microstructure and, consequently the transport properties of the GDLs. One of the key mass transport properties of the GDL that are influenced by compression is the gas permeability which is important to be determined in order to estimate the contribution of the convective flow and the distribution of saturation within the GDL [24], [25]. Also, the wettability, normally represented by the surface contact angle of the GDL, is another important characteristic that is expected to be influenced by compression, and significantly affects the dynamics of liquid water on and within the surface of the GDL.

Gostick et al. [26] investigated the in-plane and through-plane permeability of several GDL materials. The in-plane permeability was measured under different compression ratios. They found that by compressing the GDL sample to half of its initial thickness, the permeability is reduced by an order of magnitude. El-kharouf et al. [27] investigated the in-plane and through-plane permeability under different steady-state compressions using a Mercury Intrusion Porosimetry (MIP). They investigated woven and non-woven GDL materials, and found that the high fibre density of GDLs tends to lower the permeability. Also, there are a number of experimental investigations on the effect of the PTFE loading, carbon loading, microporous layer (MPL) coating and sintering on the permeability of several GDL materials [24], [25], [28]–[32]. For example, for a given PTFE loading, the permeability was found to decrease with

increasing carbon loading and this is mainly due to the increase in the thickness of the MPL [31]. Fuel cell performance wise, the benefit of the MPL becomes apparent in the intermediate current density region, i.e. the ohmic loss controlled region, since the conformability of this layer minimises the contact resistance between the GDL and the catalyst layer. Such a benefit outweighs the negative effects associated with the concentration losses controlled region, i.e. long diffusion paths and reduced mass transport properties [32].

Likewise, there have been similar investigations in the literature which attempt to correlate the wettability of the GDL to the contact resistance between the GDL and the bipolar plates [33], thermal characteristics of the GDL surface [34], PTFE loading [35][36], MPL composition [37][38] and GDL compression [23] [36]. Radhakirshnan and Haridoss [23] measured the contact angle for TGP-H-120 GDL material before and after five cycles of compression. They found that the contact angle decreases after each cycle of compression and this was attributed to the loss of PTFE particles as a result of compression. They also compared the wettability of GDLs after compression and after a 96-hour electrochemical aging. They found that the cyclic compression tends to affect the hydrophobicity of the sample more than the electrochemical aging. Kumar et al. [36] found that PTFE-treatment of the GDL material in stages reduces the hydrophobicity loss of the GDL after being subject to cyclic compression.

As demonstrated above, very few experimental works have been conducted to investigate the effect of compression on the gas permeability and the wettability of the GDL materials. Equally, previous compression tests appear to neglect the fact that the GDL inside the fuel cell is subjected to two types of compression: (i) assembling compression, arising as a result of the forces used to clamp and assemble the fuel cell components, and (ii) cyclic compression induced by the swelling (caused by the hydration) and shrinkage (caused by the dehydration) of the membrane electrolyte. The level of hydration/dehydration depends on how much water

is produced at the cathode electrode and/or the moisture content of the oxidant and fuel gases. The compression on the GDL due to swelling of the membrane could be up to 2 MPa [39]. Therefore, in this study, we experimentally investigate the through-plane permeability and the contact angle of the GDL materials, which are subjected to the above two types of compressions, in order to obtain more accurate and realistic values for the permeability and the contact angle. Subsequently, these values could be fed into the mathematical models of PEM fuel cells to obtain better model predictions of cell performance before and after compression. To the best of the authors' knowledge, there are no similar studies in the open literature.

2. Methodology

This section explains the experimental methods employed to perform compression and through-plane permeability tests on the GDL materials. Five different commercial GDL materials have been used in this investigation; Table 1 shows their properties, as provided by the manufacturers, i.e. Toray International (UK), and SGL Technologies GmbH (Germany). The morphology and the gas permeability were investigated before and after performing the compression tests. In addition, scanning electron microscope (SEM) images obtained from a JEOL instrument (Model JBM-BO10LA) have been used to investigate the morphology. SEM cross-section images were obtained by placing the samples vertically using a cross-sectional sample holder, which enables to observe the top view edges of the samples. Therefore, cross-sectional images can be obtained by observing the whole thickness of the GDL

Table 1. Manufacturers physical properties of the tested carbon paper substrates.

Manufacturer type	Initial Thickness[(a)] (µm)	PTFE Loading (%)	PTFE Loading of MPL (%)

Toray-H-90	282.5 ± 1.0	5	NA
SGL-24-BA	210 ± 3.1	5	NA
SGL-10-BA	397.5 ± 1.0	5	NA
SGL-34-BC	317.5 ± 2.4	5	25
SGL-35-BC	322.5 ± 1.0	5	25

(a) Thickness measurements are based on 95% confidence

2.1 Compression test

A universal testing machine, Shimadzu EZ-LX, was used to perform the compression tests on the investigated GDL samples. The machine was corrected for compliance as described in [40]; such a procedure ensures the mitigation of the inaccuracies associated with the estimation of the thickness of the samples undergoing the compression test. The compression test was designed in such a way that simulates an initial assembling compression of 1 MPa (0-1 MPa), followed by 10 cycles of loading and unloading in the range between 1 and 3 MPa, thus simulating the compression arising as a result of hydration/dehydration of the membrane electrolyte; this cyclic range (i.e. 1-3 MPa) must cover the extreme cases of fully dry and fully hydrated membrane electrolytes. The conservative value of 3 MPa was selected in order to cover the highest possible compression the GDL material may be subjected to inside the fuel cell. The ambient temperature and relative humidity in the laboratory at the time that the compression tests were performed were about 20°C and 40%, respectively. Fig. 1 shows the applied load on the tested GDL samples as a function of time. To conform to the size and shape of the sample holder of the gas permeability setup, the GDL samples were made circular with 25.4 mm in diameter.

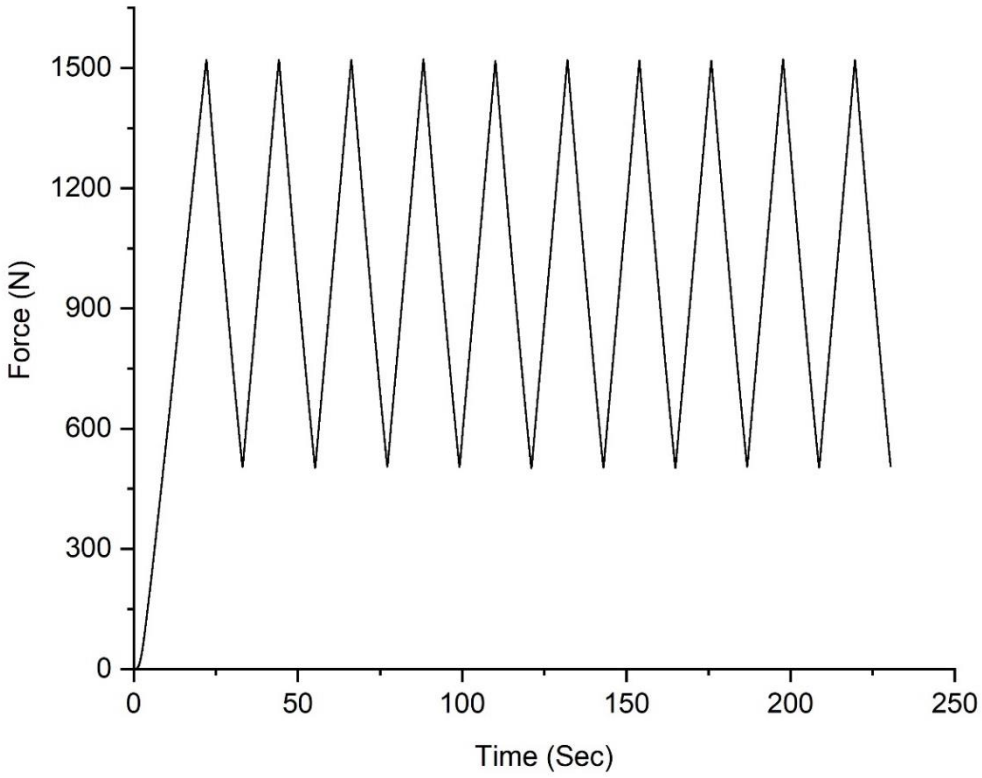

Fig. 1 Applied load as a function of the time subjected on the GDL samples during compression.

2.2 Through-plane gas permeability test

Fig. 2 shows a schematic of the in-house built setup used to estimate the through-plane permeability of the tested GDLs. As shown in Fig. 2, the setup comprises lower and upper fixtures, and a GDL sample of 25.4 mm is placed and tightened between these two fixtures [30]. Nitrogen gas is forced to flow through the sample, and measurements are taken by obtaining the pressure drop across the GDL for at least 5 flowrates. A flow controller (HFC-202, Teledyne Hastings, UK) with a range of 0.0–0.1 SLPM is used to control the flowrate of the nitrogen gas. A differential pressure sensor (PX653, Omega, UK) with a range of ±12.5 Pa, was used to measure the pressure difference across the GDL sample.

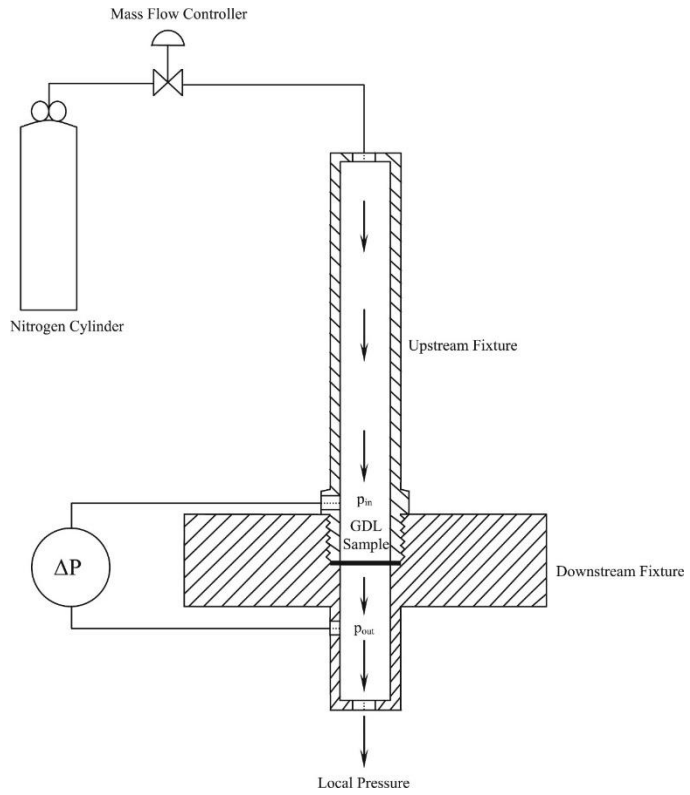

Fig. 2 A schematic of the experimental setup of the through-plane permeability. Reprinted from Ref. [36] with the permission of Elsevier.

The assumption of negligible inertial losses is valid due to the sufficiently low flow rates used. Therefore, Darcy's law could be used to calculate the gas permeability of the GDL samples, i.e.

$$\frac{\Delta P}{L} = \frac{\mu}{K} u \tag{1}$$

$$u = \frac{Q}{\pi D^2/4} \quad (2)$$

where ΔP is the pressure difference across the GDL sample, L is the measured thickness of the sample, μ is the dynamic viscosity of the flowing gas (i.e. nitrogen) which is about 1.8×10^5 Pa.s at 20 °C, K is the gas permeability of the GDL sample, u is the velocity of the flowing gas, Q is the volumetric flow rate and D is the diameter of the GDL sample. Fig. 3 shows typical pressure gradients as a function of the velocity of the flowing gas for: (a) Toray-H-90 (uncoated) and (b) SGL-34-BC (MPL-coated). As it could be seen from the figure, different ranges of gas flow rates were used for the presented GDL materials. The reason behind this is that the SGL GDL material (i.e. 34BC) is MPL-coated and therefore it is much more resistive to the transport of the flowing gas compared to the uncoated GDL material of Toray-H-90. To this end, much lower flow rates must be used when testing SGL 34BC in order not to exceed the maximum limit of the pressure sensor which is as low as 12.5 Pa. The presented set of data are measured before and after the compression of 5 samples of each GDL material. The error bars represent the 95% confidence intervals. The data were linearly curve-fitted to obtain the slope of the curve, i.e. $\frac{\mu}{K}$, and subsequently calculate the gas permeability of the GDL material.

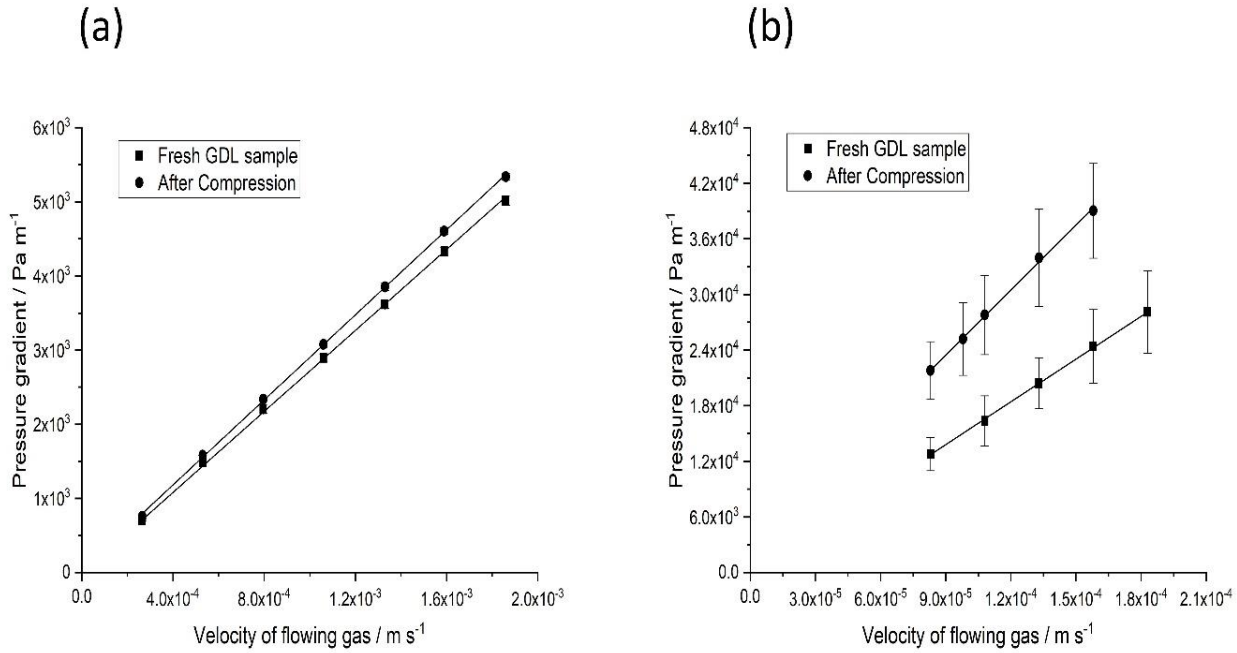

Fig. 3 The pressure gradient as a function of the flowing gas velocity for (a) Toray-H-90 and (b) SGL-34-BC before and after compression.

2.3 Contact angle test

A video drop shape system FTA200 goniometer (First Ten Angstroms, USA) was used to measure the water contact angle of the GDL surface.

As the surface of the GDL is highly inhomogeneous, the contact angle measurement needs to be performed at as many positions of the GDL sample as possible in order to obtain a realistic average value of the contact angle. In this work, the contact angle was measured at 10 positions of the GDL sample and the average value and the 95% confidence interval were then calculated.

3. Results and discussion

3.1 Stress-strain curves

The mechanical characterisation of the tested GDLs is presented in the form of stress-strain curves. Fig. 4 shows typical stress-strain curves of (a) uncoated Toray-H-90 and (b) MPL-

208 coated SGL-34-BC GDL samples. All the stress-strain curves of the tested GDL samples
209 demonstrate the same trend: hysteresis, i.e. the difference between the forward curve (loading)
210 and backward curve (unloading), is significant for the first cycle and then becomes much less
211 significant for the subsequent cycles. This implies that the very first compression caused by
212 the assembly of the fuel cell is responsible for most of the deformation of the GDL. Subsequent
213 cycles of the compression (or loading), due to the membrane hydration and non-compression
214 (i.e. unloading) due to the membrane dry-out contributes much less to the GDL deformation.
215 Although not clear from Fig. 4, the reduced thickness of the uncoated GDL materials (i.e.
216 Toray-H-90, SGL-10-BA, SGL-24-BA) tend to saturate faster than those of the coated GDL
217 materials (i.e. SGL-34-BC and SGL-35-BC). To elaborate further on this point, Fig. 5 was
218 generated, and it shows the relative change in the strain from one cycle to another at 1.5 MPa
219 for the uncoated Toray-H-90 and the MPL-coated SGL-34-BC GDL materials. It could be
220 inferred from the latter figure that the MPL-coated GDL materials show slightly more
221 mechanical resistance to deformation than the uncoated GDL materials. This is evidenced from
222 the observation that the thickness of the uncoated Toray-H-90 visually becomes saturated after
223 the 8^{th} cycle whereas the MPL-coated SGL-34 BC GDL appear to be visually saturated after
224 the 9^{th} cycle. This observation is in accordance with the idea that the addition of MPL to the
225 GDL improves the mechanical resistance of the GDL [18], [30], [40], [41].

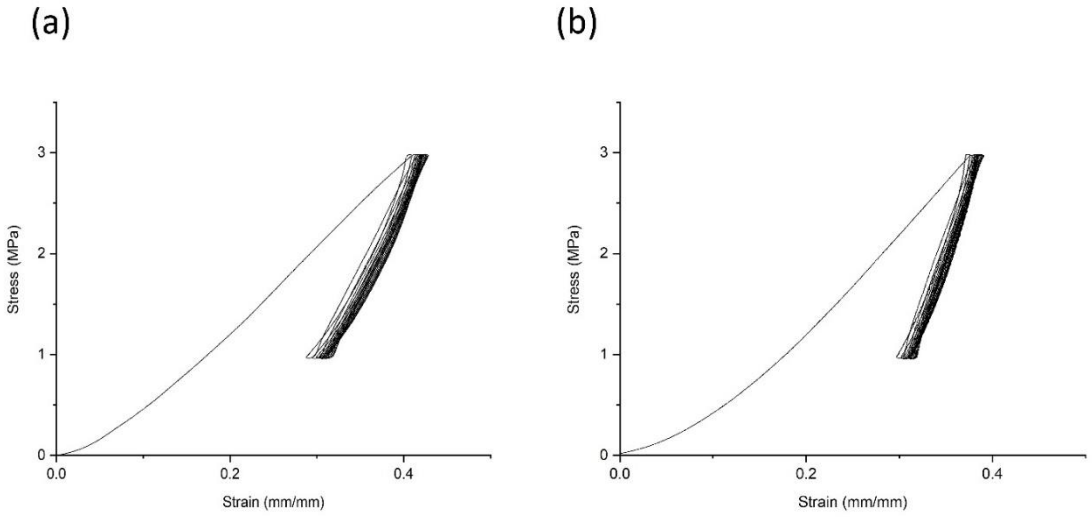

226

227 **Fig. 4 The steady-state and cyclic compression stress-strain relationship of (a) Toray-H-90 and (b) SGL-34-**
228 **BC.**

229

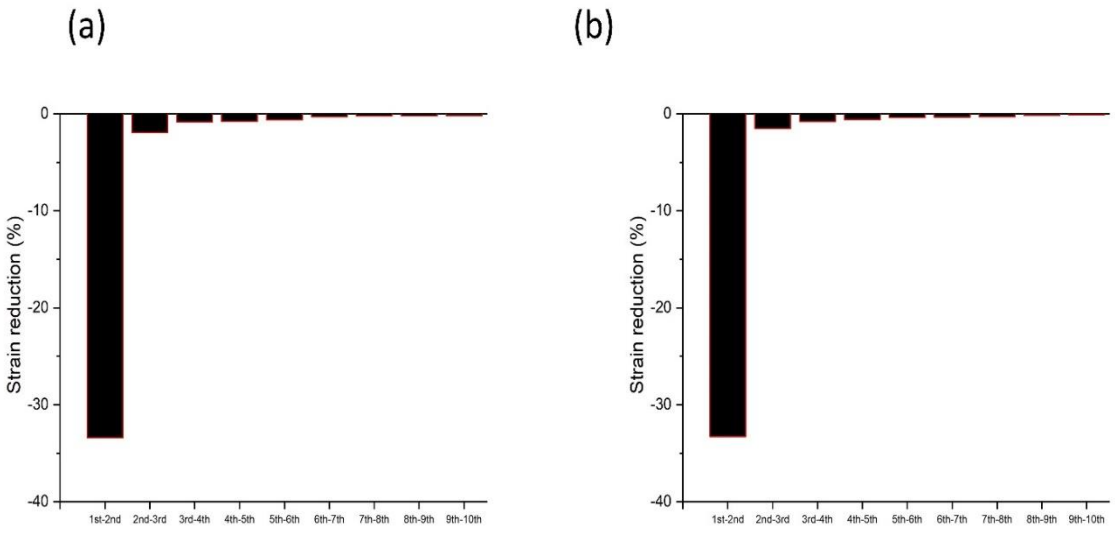

230

231 **Fig. 5 The percentage difference of the strain at 1.5 MPa for all the compression cycles of (a) Toray-H-90 and**
232 **(b) SGL-34-BC.**

233 ## 3.2. Gas permeability

234 Table 3 shows the through-plane permeability values of the tested GDL materials before and
235 after compression. It is observed from the latter table that there exists a correlation between the
236 reduction in thickness and the reduction in the gas permeability for either the uncoated and

MPL-coated GDL materials: as the reduction in thickness increases, the reduction in the through-plane permeability increases. The reduction in the thickness of the GDL, caused by compression signals that the porosity of the GDL decreases. Subsequently, the gas permeability, which is a strong function of the porosity, as evidenced from the Kozney-Carman equation [26], decreases.

Table 2. Through-plane permeability before and after compression, and the percentage of both reduction in thickness and permeability.

GDL Type	Through-plane permeability before compression (m^2)	Through-plane permeability after compression (m^2)	Reduction in thickness (%)	Reduction in permeability (%)
Toray-H-90	$(6.62 \pm 0.10) \times 10^{-12}$	$(6.22 \pm 0.06) \times 10^{-12}$	3.5	5.0
SGL-24-BA	$(1.50 \pm 0.04) \times 10^{-11}$	$(1.08 \pm 0.02) \times 10^{-11}$	21.4	27.9
SGL-10-BA	$(2.38 \pm 0.13) \times 10^{-11}$	$(1.31 \pm 0.08) \times 10^{-11}$	28.3	45.1
SGL-34-BC	$(1.20 \pm 0.19) \times 10^{-13}$	$(7.19 \pm 1.23) \times 10^{-14}$	10.9	39.6
SGL-35-BC	$(2.74 \pm 0.22) \times 10^{-13}$	$(7.33 \pm 1.17) \times 10^{-14}$	31.0	73.3

To elaborate more on how the structure and thickness change with compression, cross-sectional SEM images of the tested uncoated and MPL-coated GDL materials have been generated, see Fig. 6 and Fig. 7. It is seen from the latter figures that the original thicknesses of the tested GDLs have, in general, reduced after performing the compression test. Notably, the difference in the thickness of Toray-H-90 before and after compression is very small, see Fig. 6(a-b). This observation is in line with the relatively small value reported in Table 3 for the reduction in thickness of the above mentioned GDL material, i.e. 3.5%. The high resistance to deformation (or compliance) shown by Toray-H-90 GDL could be attributed to its relatively high density of carbon fibres compared to those of SGL-10-BA and SGL-24-BA GDLs; see Fig.8. This observation is in accordance with the density and porosity values reported for the above GDL materials [27], [28], [42]. Namely, the density and porosity of

255 Toray-H-90 (i.e. 0.45 g cm^{-3} and 0.62) are respectively higher and lower than those of SGL-
256 10-BA (0.21 g cm^{-3} and 0.88), and SGL-24-BA (i.e. 0.28 g cm^{-3} and 0.74), thus imparting a
257 higher degree of stiffness to the Toray GDL material. Equally, compared to Toray-H-90 and
258 SGL-24-BA GDLs, SGL-10-BA GDL material shows the highest level of reduction in
259 thickness and gas permeability as it has the lowest density and the highest porosity,
260 respectively.

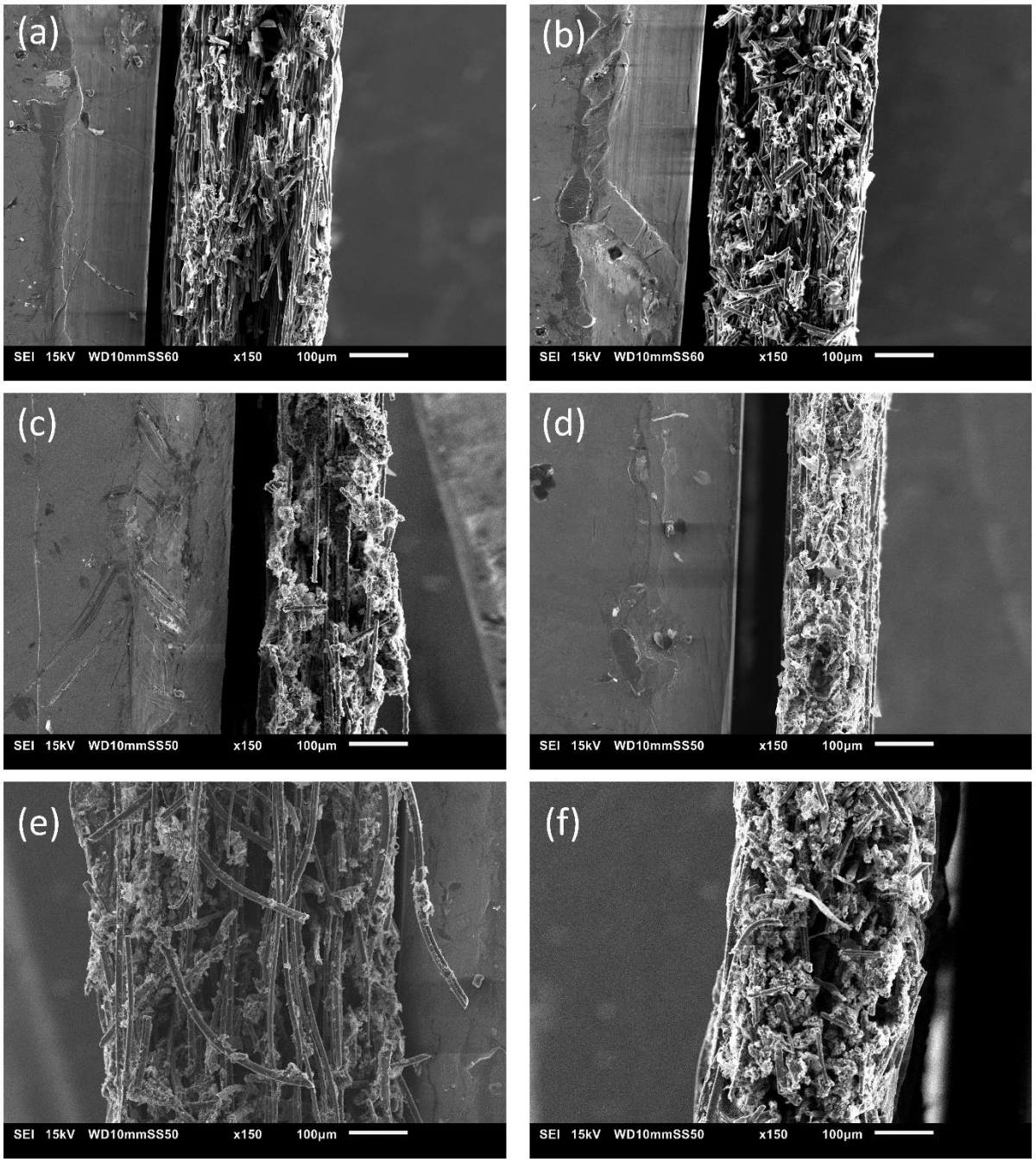

261

262 **Fig. 6 Cross-sectional SEM images at a magnification of 150x for uncoated GDL samples before and after**
263 **compression, (a) uncompressed Toray-H-90 (b) Compressed Toray-H-90 (c) Uncompressed SGL-24-BA (d)**
264 **Compressed SGL-24-BA (e) Uncompressed SGL-10-BA (f) Compressed SGL-10-BA.**

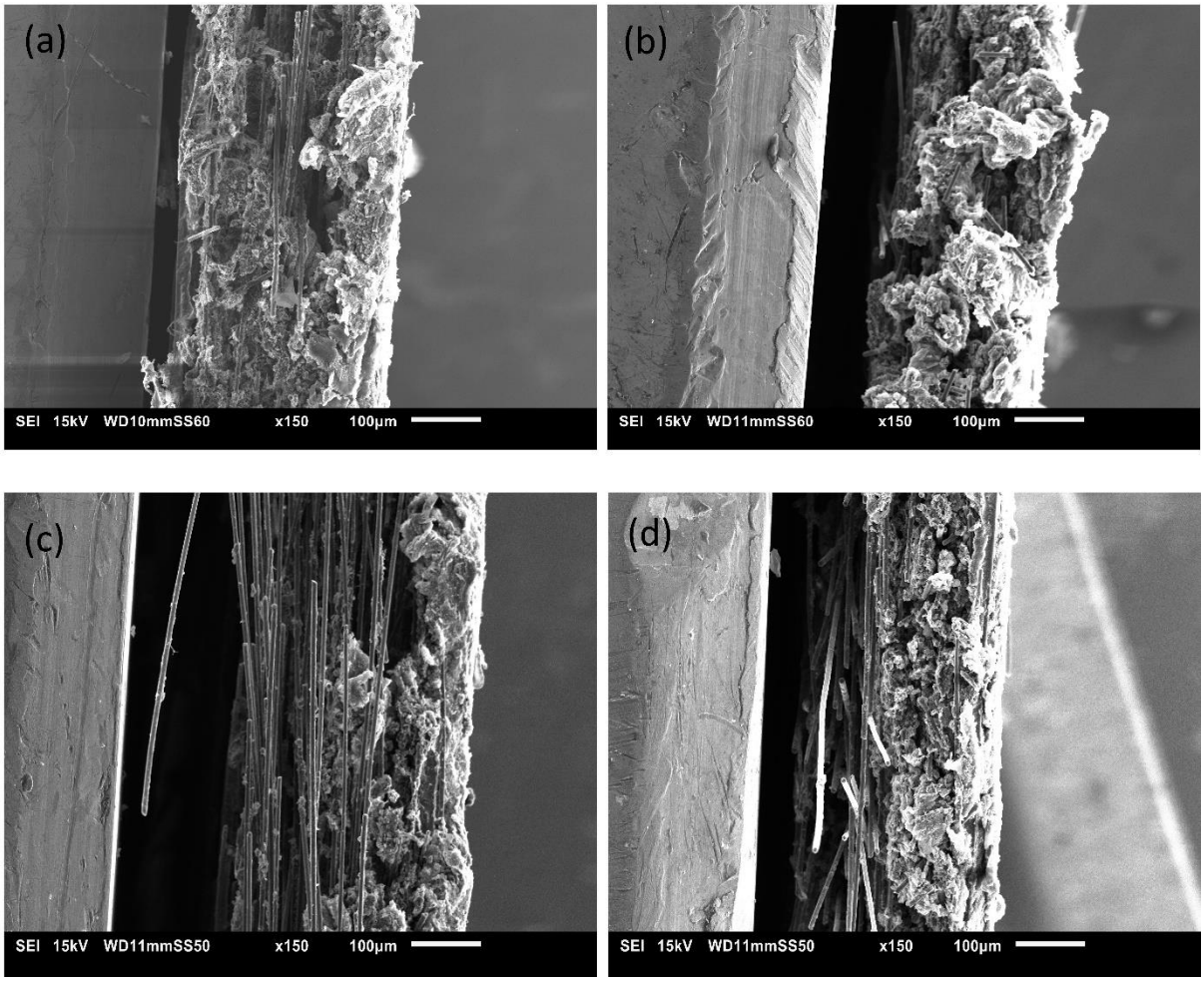

Fig. 7 Cross-sectional SEM images at a magnification of 150x for MPL-coated GDL samples before and after compression, (a) uncompressed SGL-34-BC (b) compressed SGL-34-BC (c) uncompressed SGL-35-BC (d) compressed SGL-35-BC.

As for the MPL-coated GDLs (i.e. SGL-34-BC and SGL-35-BC), the respective cross-sectional SEM images in Fig. 7 show that the degree of MPL penetration into the carbon substrate of SGL-35-BC GDL after compression is more significant than that of SGL-34-BC GDL. This could be attributed to the higher porosity of SGL-35-BC (i.e. ~ 0.53) compared to that of SGL-34-BC GDL (i.e. ~ 0.48) [27]. The MPL is significantly less porous and, subsequently, less permeable than the carbon substrate [30], and therefore there is a higher degree of MPL penetration into the carbon substrate and this results in higher levels of reduction in the thickness and gas permeability of the entire GDL sandwich. This interprets the result that the reduction in thickness and gas permeability of SGL-35-BC, characterised by more MPL-penetration after compression, is significantly higher than that of SGL-34-BC.

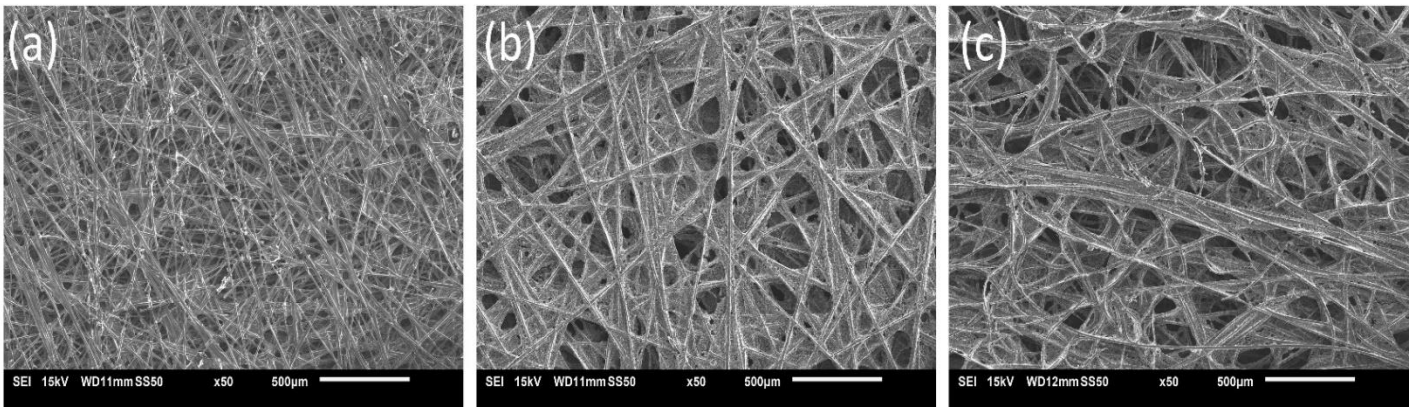

Fig. 8 SEM image for the surface of the tested uncoated GDLs (a) Toray-H-90 (b) SGL-24-BA and (c) SGL-10-BA.

279

280

281 3.3. Wettability of GDLs

282 Table 3 lists the values of the contact angle of the tested GDLs before and after compression.
283 As expected, the surfaces of all the tested GDL materials, either before or after compression,
284 were found to be hydrophobic (the respective contact angles are all greater than 90°). The
285 contact angle changes with the roughness of the surface; the rougher is the surface, the greater
286 is the surface contact angle [27]. Typically, internal contact angle of GDLs corresponds to the
287 pore connections of the carbon fibres used, however the external contact angle (i.e. surface
288 contact angle) reflects the overall surface morphology and the roughness of the tested surface.
289 Therefore, we can notice that external contact angles often show higher values than internal
290 contact angles of GDLs [43].One may see from Table 3 that the contact angles of all the tested
291 GDL materials reduce after compression. Also, Fig. 9 clearly shows that the contact angle for
292 one of the SGL-34-BC GDL samples before compression is greater than that after compression.
293 The reason behind this reduction in the contact angle after compression is that the surface of
294 the GDL sample becomes smoother after compression, as evidenced from the cross-section
295 images of the tested GDL materials shown in Fig.6 and Fig.7. This is corroborated with the

results that show that the contact angle of the GDL surface generally reduces as the surface roughness decreases [44].

Table 3. Contact angle measurements of the tested GDL materials before and after compression.

GDL Manufacturer type	Contact angle before compression (°)	Contact angle after compression (°)
Toray-H-90	123.7 ± 3.3	120.3 ± 3.3
SGL-24-BA	123.8 ± 3.3	120.2 ± 2.5
SGL-10-BA	126.1 ± 3.5	113.7 ± 2.0
SGL-34-BC	126.7 ± 3.4	112.8 ± 1.9
SGL-35-BC	122.1 ± 4.1	115.0 ± 3.9

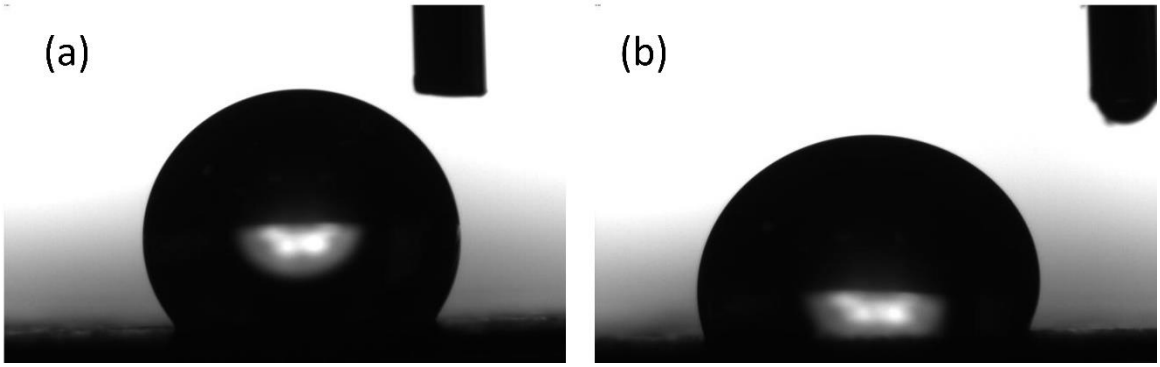

Fig. 9 Water droplet on the GDL surface of SGL-34-BC (a) before compression and (b) after compression.

4. Conclusions

In this study, different types of GDL materials were ex-situ compressed using a universal testing machine. The compression test was designed in such a way that simulates an initial assembling compression, followed by a number of cycles of loading and unloading, thus simulating the compression arising as a result of hydration/dehydration of the membrane. The thickness, the through-plane permeability, the contact angle, and the morphology of the tested GDL materials were examined before and after performing the compression test. The obtained values of the above variables after compression are of use for PEFC models as they are more realistic and subsequently enhance the predictions of the models. The following are the main findings of the study;

- The coated GDL materials appear to be slightly more resistive to deformation than the uncoated GDL materials, and this is due to the enhanced mechanical strength of the coated GDLs as a result of the addition of relatively dense material, i.e. the MPL, to the carbon substrate.
- The tested Toray carbon substrate is mechanically stronger than the tested SGL carbon substrates and this is due to the higher density and lower porosity demonstrated by the former carbon substrate. This translates into a smaller reduction in thickness and gas permeability for the Toray carbon substrate after performing the compression test.
- One of the tested coated GDL materials (i.e. SGL-35-BC) shows substantially much higher reduction in thickness and gas permeability compared to the other tested coated GDL material (i.e. SGL-34-BC). This is attributed to the higher level of MPL penetration demonstrated by the former coated GDL material.

- The contact angle of all the tested GDL materials were found to decrease by about 3°-15° after compression, and this is due to the increased surface smoothness after compression.

Acknowledgements

The first author would like to acknowledge and appreciate the financial support from the Kuwait Institute for Scientific Research (KISR). Also, a grateful acknowledgement to Mr Jonathon Woods for his technical assistance and support when using the Shimadzu EZ-LX universal testing machine.

346 ## References

347 [1] P. Rama, R. Chen, and J. Andrews, "A review of performance degradation and failure
348 modes for hydrogen-fuelled polymer electrolyte fuel cells," *Proc. Inst. Mech. Eng. Part*
349 *A J. Power Energy*, vol. 222, no. 5, pp. 4214–441, 2008.

350 [2] C. Wang, M. Waje, X. Wang, J. M. Tang, R. C. Haddon, and Y. S. Yan, "Proton exchange
351 membrane fuel cells with carbon nanotube based electrodes," *Nano Lett.*, vol. 4, no. 2,
352 pp. 345–348, 2004.

353 [3] H. Zamora, P. Cañizares, M. A. Rodrigo, and J. Lobato, "Improving of micro porous
354 layer based on advanced carbon materials for high temperature proton exchange
355 membrane fuel cell electrodes," *Fuel Cells*, vol. 15, no. 2, pp. 375–383, 2015.

356 [4] S. Litster and G. McLean, "PEM fuel cell electrodes," *J. Power Sources*, vol. 130, no. 1–
357 2, pp. 61–76, 2004.

358 [5] X.-Z. Yuan and H. Wang, "PEM Fuel Cell Fundamentals," in *PEM Fuel Cell*
359 *Electrocatalysts and Catalyst Layers*, London: Springer London, 2008, pp. 1–87.

360 [6] S. Subramaniam, G. Rajaram, K. Palaniswamy, and V. R. Jothi, "Comparison of
361 perforated and serpentine flow fields on the performance of proton exchange membrane
362 fuel cell," *J. Energy Inst.*, vol. 90, no. 3, pp. 363–371, 2017.

363 [7] S. Latorrata, C. Cristiani, and G. Dotelli, "Performance Evaluation and Durability
364 Enhancement of FEP-Based Gas Diffusion Media for PEM Fuel Cells," *Energies*, vol.
365 10, no. 12, p. 17, 2017.

366 [8] J. Park, H. Oh, T. Ha, Y. Il Lee, and K. Min, "A review of the gas diffusion layer in
367 proton exchange membrane fuel cells: Durability and degradation," *Appl. Energy*, vol.
368 155, pp. 866–880, 2015.

369 [9] J. Millichamp, T. J. Mason, T. P. Neville, N. Rajalakshmi, R. Jervis, P. R. Shearing, and
370 D. J. L. Brett, "Mechanisms and effects of mechanical compression and dimensional
371 change in polymer electrolyte fuel cells - A review," *J. Power Sources*, vol. 284, pp.
372 305–320, 2015.

373 [10] J. Ge, A. Higier, and H. Liu, "Effect of gas diffusion layer compression on PEM fuel cell
374 performance," *J. Power Sources*, vol. 159, no. 2, pp. 922–927, 2006.

375 [11] S. S. L. Rao, A. Shaija, and S. Jayaraj, "Performance analysis of a transparent PEM fuel

376 cell at theoptimized clamping pressure applied on its bolts," in *Materials Today:*
377 *Proceedings*, 2018, vol. 5, no. 1, pp. 58–65.

378 [12] A. H. Mahmoudi, A. Ramiar, and Q. Esmaili, "Effect of inhomogeneous compression of
379 gas diffusion layer on the performance of PEMFC with interdigitated flow field," *Energy*
380 *Convers. Manag.*, vol. 110, pp. 78–89, 2016.

381 [13] T. J. Mason, J. Millichamp, T. P. Neville, A. El-Kharouf, B. G. Pollet, and D. J. L. Brett,
382 "Effect of clamping pressure on ohmic resistance and compression of gas diffusion
383 layers for polymer electrolyte fuel cells," *J. Power Sources*, vol. 219, pp. 52–59, 2012.

384 [14] J. Wang, J. Yuan, and B. Sundén, "On electric resistance effects of non-homogeneous
385 GDL deformation in a PEM fuel cell," *Int. J. Hydrogen Energy*, vol. 42, no. 47, pp.
386 28537–28548, 2017.

387 [15] S. Tanaka and T. Shudo, "Experimental and numerical modeling study of the electrical
388 resistance of gas diffusion layer-less polymer electrolyte membrane fuel cells," *J. Power*
389 *Sources*, vol. 278, pp. 382–395, 2015.

390 [16] C. J. Netwall, B. D. Gould, J. A. Rodgers, N. J. Nasello, and K. E. Swider-Lyons,
391 "Decreasing contact resistance in proton-exchange membrane fuel cells with metal
392 bipolar plates," *J. Power Sources*, vol. 227, pp. 137–144, 2013.

393 [17] P. Liang, D. Qiu, L. Peng, P. Yi, X. Lai, and J. Ni, "Contact resistance prediction of
394 proton exchange membrane fuel cell considering fabrication characteristics of metallic
395 bipolar plates," *Energy Convers. Manag.*, vol. 169, no. April, pp. 334–344, 2018.

396 [18] S. Escribano, J. F. Blachot, J. Ethève, A. Morin, and R. Mosdale, "Characterization of
397 PEMFCs gas diffusion layers properties," *J. Power Sources*, vol. 156, no. 1 SPEC. ISS.,
398 pp. 8–13, 2006.

399 [19] X. Q. Xing, K. W. Lum, H. J. Poh, and Y. L. Wu, "Optimization of assembly clamping
400 pressure on performance of proton-exchange membrane fuel cells," *J. Power Sources*,
401 vol. 195, no. 1, pp. 62–68, 2010.

402 [20] N. De Las Heras, E. P. L. Roberts, R. Langton, and D. R. Hodgson, "A review of metal
403 separator plate materials suitable for automotive PEM fuel cells," *Energy Environ. Sci.*,
404 vol. 2, no. 2, pp. 206–214, 2009.

405 [21] W. Yoon, X. Huang, P. Fazzino, K. L. Reifsnider, and M. A. Akkaoui, "Evaluation of

406 coated metallic bipolar plates for polymer electrolyte membrane fuel cells," *J. Power*
407 *Sources*, vol. 179, no. 1, pp. 265–273, 2008.

408 [22] P. A. Gigos, Y. Faydi, and Y. Meyer, "Mechanical characterization and analytical
409 modeling of gas diffusion layers under cyclic compression," *Int. J. Hydrogen Energy*,
410 vol. 40, no. 17, pp. 5958–5965, 2015.

411 [23] V. Radhakrishnan and P. Haridoss, "Effect of cyclic compression on structure and
412 properties of a Gas Diffusion Layer used in PEM fuel cells," *Int. J. Hydrogen Energy*,
413 vol. 35, no. 20, pp. 11107–11118, 2010.

414 [24] O. M. Orogbemi, D. B. Ingham, M. S. Ismail, K. J. Hughes, L. Ma, and M.
415 Pourkashanian, "On the gas permeability of the microporous layer used in polymer
416 electrolyte fuel cells," *J. Energy Inst.*, vol. 41, no. 46, pp. 21345–21351, 2017.

417 [25] O. M. Orogbemi, D. B. Ingham, M. S. Ismail, K. J. Hughes, L. Ma, and M.
418 Pourkashanian, "Through-plane gas permeability of gas diffusion layers and
419 microporous layer: Effects of carbon loading and sintering," *J. Energy Inst.*, vol. 91, no.
420 2, pp. 270–278, 2018.

421 [26] J. T. Gostick, M. W. Fowler, M. D. Pritzker, M. A. Ioannidis, and L. M. Behra, "In-plane
422 and through-plane gas permeability of carbon fiber electrode backing layers," *J. Power*
423 *Sources*, vol. 162, no. 1, pp. 228–238, 2006.

424 [27] A. El-Kharouf, T. J. Mason, D. J. L. Brett, and B. G. Pollet, "Ex-situ characterisation of
425 gas diffusion layers for proton exchange membrane fuel cells," *J. Power Sources*, vol.
426 218, pp. 393–404, 2012.

427 [28] M. S. Ismail, T. Damjanovic, K. Hughes, D. B. Ingham, L. Ma, M. Pourkashanian, and
428 M. Rosli, "Through-Plane Permeability for Untreated and PTFE-Treated Gas Diffusion
429 Layers in Proton Exchange Membrane Fuel Cells," *J. Fuel Cell Sci. Technol.*, vol. 7, no.
430 5, p. 51016, 2010.

431 [29] M. S. Ismail, T. Damjanovic, D. B. Ingham, L. Ma, and M. Pourkashanian, "Effect of
432 polytetrafluoroethylene-treatment and microporous layer-coating on the in-plane
433 permeability of gas diffusion layers used in proton exchange membrane fuel cells," *J.*
434 *Power Sources*, vol. 195, no. 19, pp. 6619–6628, 2010.

435 [30] M. S. Ismail, D. Borman, T. Damjanovic, D. B. Ingham, and M. Pourkashanian, "On the

436 through-plane permeability of microporous layer-coated gas diffusion layers used in
437 proton exchange membrane fuel cells," *Int. J. Hydrogen Energy*, vol. 36, no. 16, pp.
438 10392–10402, 2010.

439 [31] O. M. Orogbemi, D. B. Ingham, M. S. Ismail, K. J. Hughes, L. Ma, and M.
440 Pourkashanian, "The effects of the composition of microporous layers on the
441 permeability of gas diffusion layers used in polymer electrolyte fuel cells," *Int. J.*
442 *Hydrogen Energy*, vol. 41, no. 46, pp. 21345–21351, 2016.

443 [32] M. S. Ismail, K. . Hughes, D. B. Ingham, L. Ma, and M. Pourkashanian, "Effect of PTFE
444 loading of gas diffusion layers on the performance of proton exchange membrane fuel
445 cells running at high-efficiency operating conditions," *Int. J. ENERGY Res.*, vol. 37, no.
446 13, pp. 1592–1599, 2013.

447 [33] M. S. Ismail, D. B. Ingham, L. Ma, and M. Pourkashanian, "The contact resistance
448 between gas diffusion layers and bipolar plates as they are assembled in proton exchange
449 membrane fuel cells," *Renew. Energy*, vol. 52, pp. 40–45, 2013.

450 [34] O. A. Obeisun, D. P. Finegan, E. Engebretsen, J. B. Robinson, O. O. Taiwo, G. Hinds, P.
451 R. Shearing, and D. J. L. Brett, "Ex-situ characterisation of water droplet dynamics on
452 the surface of a fuel cell gas diffusion layer through wettability analysis and thermal
453 characterisation," *Int. J. Hydrogen Energy*, vol. 42, no. 7, pp. 4404–4414, 2017.

454 [35] T. Chen, S. Liu, J. Zhang, and M. Tang, "Study on the characteristics of GDL with
455 different PTFE content and its effect on the performance of PEMFC," *Int. J. Heat Mass*
456 *Transf.*, vol. 128, pp. 1168–1174, 2019.

457 [36] R. John Felix Kumar, V. Radhakrishnan, and P. Haridoss, "Enhanced mechanical and
458 electrochemical durability of multistage PTFE treated gas diffusion layers for proton
459 exchange membrane fuel cells," *Int. J. Hydrogen Energy*, vol. 37, no. 14, pp. 10830–
460 10835, 2012.

461 [37] J. H. Chun, D. H. Jo, S. G. Kim, S. H. Park, C. H. Lee, and S. H. Kim, "Improvement of
462 the mechanical durability of micro porous layer in a proton exchange membrane fuel
463 cell by elimination of surface cracks," *Renew. Energy*, vol. 48, pp. 35–41, 2012.

464 [38] A. Ozden, S. Shahgaldi, X. Li, and F. Hamdullahpur, "A graphene-based microporous
465 layer for proton exchange membrane fuel cells: Characterization and performance
466 comparison," *Renew. Energy*, vol. 126, pp. 485–494, 2018.

[39] V. V. Atrazhev, T. Y. Astakhova, D. V. Dmitriev, N. S. Erikhman, V. I. Sultanov, T. Patterson, and S. F. Burlatsky, "The Model of Stress Distribution in Polymer Electrolyte Membrane," *J. Electrochem. Soc.*, vol. 160, no. 10, pp. F1129–F1137, 2013.

[40] M. S. Ismail, A. Hassanpour, D. B. Ingham, L. Ma, and M. Pourkashanian, "On the compressibility of gas diffusion layers in proton exchange membrane fuel cells," *Fuel Cells*, vol. 12, no. 3, pp. 391–397, 2012.

[41] S. G. Kandlikar, M. L. Garofalo, and Z. Lu, "Water management in a PEMFC: Water transport mechanism and material degradation in gas diffusion layers," *Fuel Cells*, vol. 11, no. 6, pp. 814–823, 2011.

[42] A. El-Kharouf and R. Steinberger-Wilckens, "The Effect of Clamping Pressure on Gas Diffusion Layer Performance in Polymer Electrolyte Fuel Cells," *Fuel Cells*, vol. 15, no. 6, pp. 802–812, 2015.

[43] V. Gurau, M. J. Bluemle, E. S. De Castro, Y. M. Tsou, J. A. Mann, and T. A. Zawodzinski, "Characterization of transport properties in gas diffusion layers for proton exchange membrane fuel cells. 1. Wettability (internal contact angle to water and surface energy of GDL fibers)," *J. Power Sources*, vol. 160, no. 2 SPEC. ISS., pp. 1156–1162, 2006.

[44] L. Chen, H. Luan, Y. L. He, and W. Q. Tao, "Effects of roughness of gas diffusion layer surface on liquid water transport in micro gas channels of a proton exchange membrane fuel cell," *Numer. Heat Transf. Part A Appl.*, vol. 62, no. 4, pp. 295–318, 2012.